AIAA SciTech 2104

AIAA 2014-0558

Cart3D Simulations for the First AIAA Sonic Boom Prediction Workshop

Michael J. Aftosmis
Applied Modeling & Simulations Branch
NASA Ames Research Center
Moffett Field, CA 94035
michael.aftosmis@nasa.gov

Marian Nemec
Science and Technology Corp.
Applied Modeling & Simulations Branch
Moffett Field, CA 94035
marian.nemec@nasa.gov

13-17 Jan 2014, National Harbor, Maryland, USA

Introduction – Cart3D

Meshing:
- Multi-level Cartesian mesh with embedded boundaries
- Insensitive to geometric complexity
- Adjoint-based mesh adaptation

Inviscid flow solver
- Monotone second-order upwind method
- Tensor slope limiters preserve k-exactness
- Runge-Kutta with multigrid acceleration
- Domain decomposition for scalability

Output-based mesh adaptation
- Duality-preserving discrete adjoint
- Provides output correction & error estimate
- Adjoint-based mesh refinement using remaining error

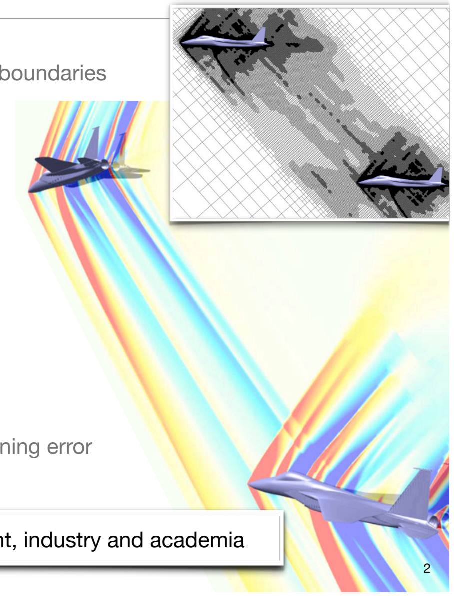

Broad use throughout NASA, US Government, industry and academia

Boom problems with Cartesian Mesh Methods

Goal: Accurate prediction of near/mid-field pressure signatures

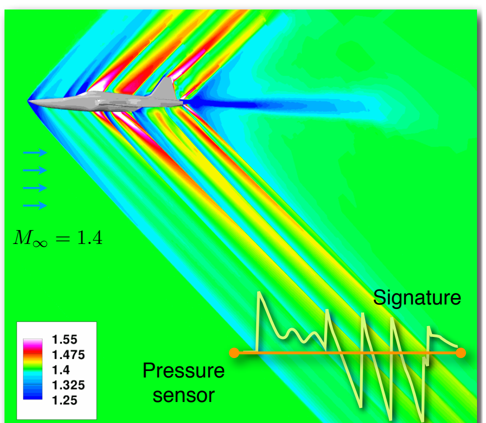

AIAA 2008-6593, Wintzer et al.

Boom problems with Cartesian Mesh Methods

Goal: Accurate prediction of near/mid-field pressure signatures

- Mesh adaptation to pressure sensor output

$$\mathcal{J}_{\text{sensor}} = \int_0^L \frac{(p - p_\infty)^2}{p_\infty} dl$$

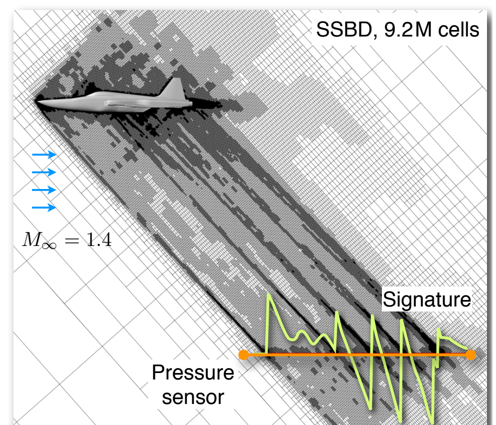

AIAA 2008-6593, Wintzer et al.

Boom problems with Cartesian Mesh Methods

Goal: Accurate prediction of near/mid-field pressure signatures

- Mesh adaptation to pressure sensor output

$$\mathcal{J}_{\text{sensor}} = \int_0^L \frac{(p - p_\infty)^2}{p_\infty} dl$$

- Mesh rotation to ~Mach angle
- Mesh stretching along dominant direction of wave propagation
- See: *AIAA 2008-0725, 6593 & AIAA 2013-0649*

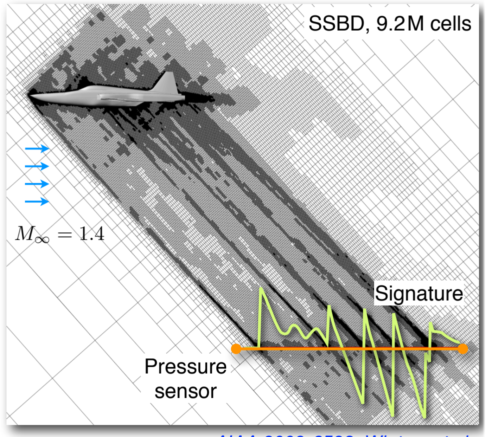

AIAA 2008-6593, Wintzer et al.

Assessing Mesh Convergence

Adjoint-based error-estimation and mesh adaptation

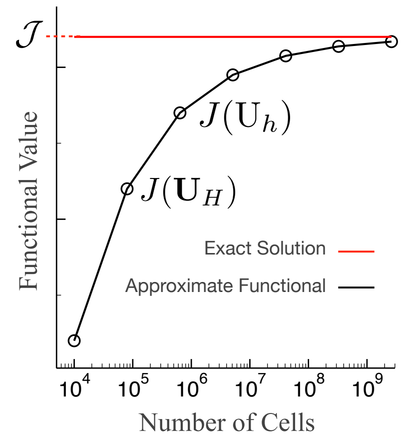

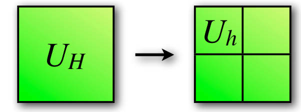

- The output asymptotically approaches its true value as the mesh is refined from $H \to h$

Assessing Mesh Convergence

Adjoint-based error-estimation and mesh adaptation

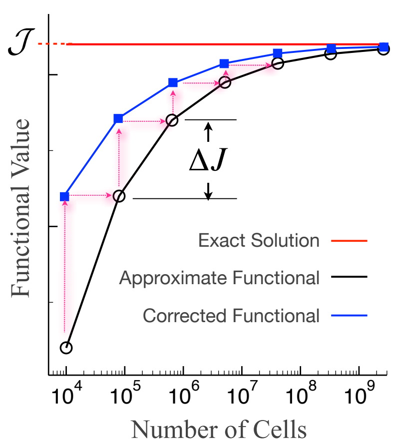

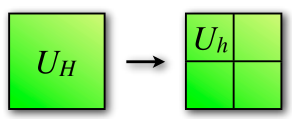

- The output asymptotically approaches its true value as the mesh is refined from $H \to h$
- Adjoint Correction: The adjoint provides a correction which predicts the value of the solution on the next mesh $J(U_h)$
- |ΔJ| vanishes with convergence

Assessing Mesh Convergence

Adjoint-based error-estimation and mesh adaptation

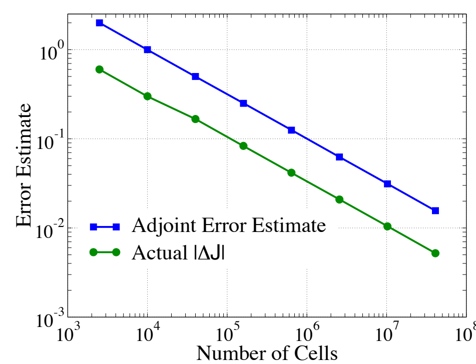

- |ΔJ| vanishes with convergence
- Error Estimate: The adjoint provides an estimate of the error remaining in the functional which sharpens with mesh convergence
- Asymptotic convergence appears linear on log-log paper
- The error estimate should bound |ΔJ|

Nomenclature

Cylindrical coordinates used for sonic boom

x : Distance along sensor (axial distance)

h : Distance from axis (radius)

Φ : Off-track angle (azimuth)

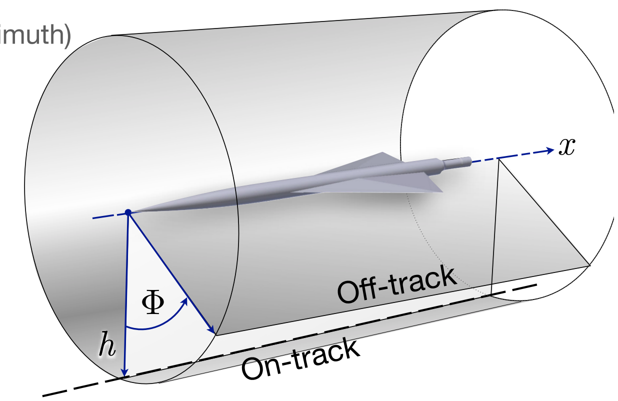

Results and Investigations

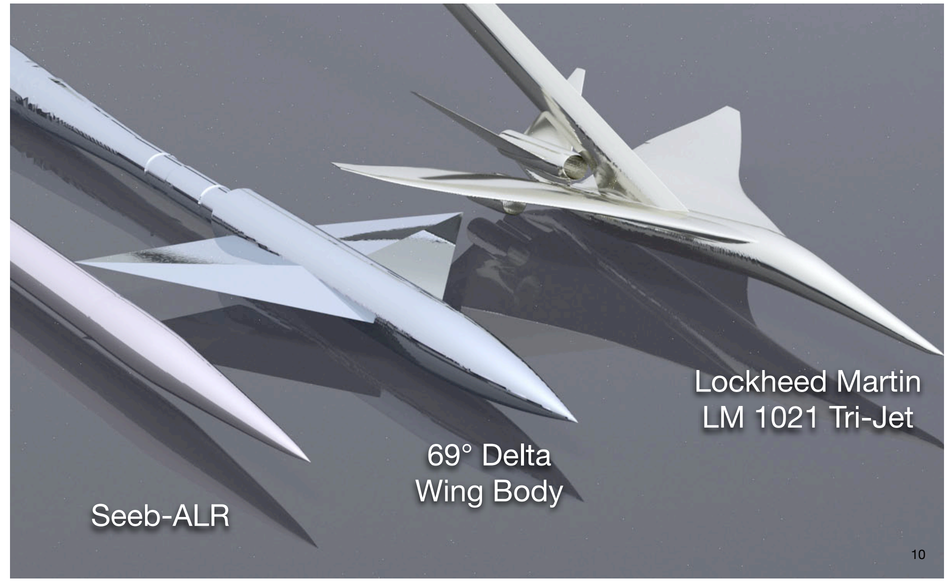

Results and Investigations

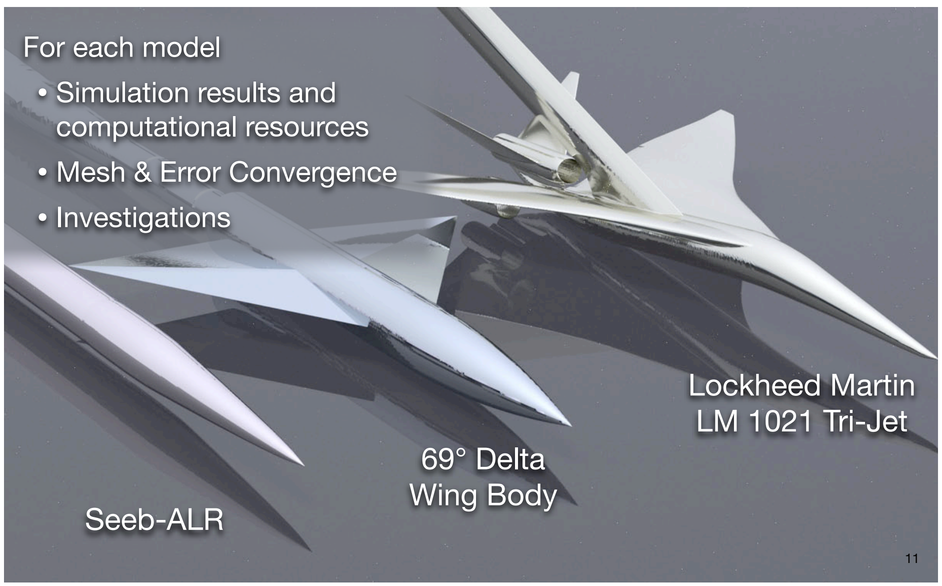

Case 1 – Seeb-ALR

$M_\infty = 1.6,\ \alpha = 0°$

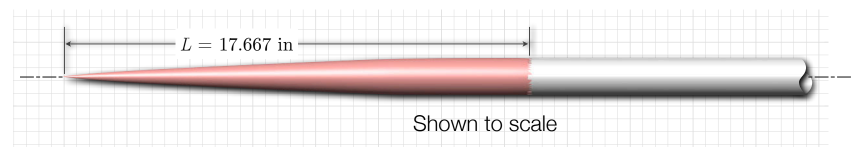

Case 1 – Seeb-ALR

$M_\infty = 1.6, \alpha = 0°$

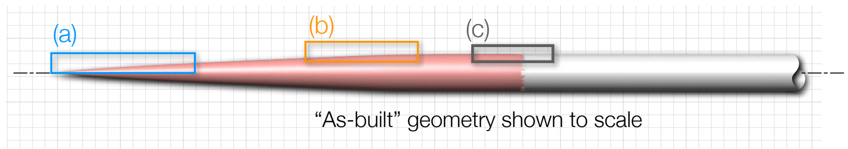

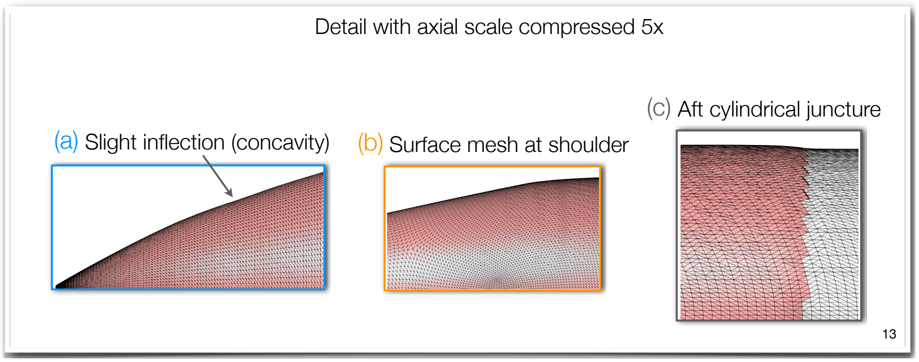

Seeb-ALR: Meshing

$M_\infty = 1.6, \alpha = 0°$, On-track @ $h = 21.2$ in. & 42 in.

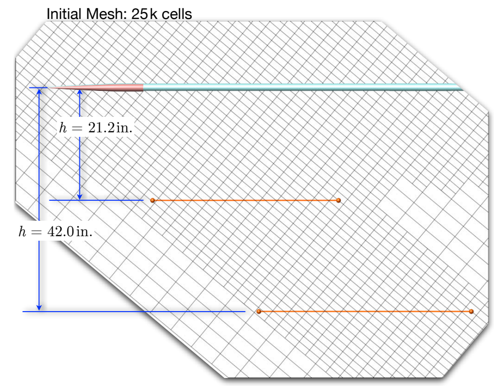

Seeb-ALR: Meshing

$M_\infty = 1.6, \alpha = 0°$, On-track @ $h = 21.2$ in. & 42 in.

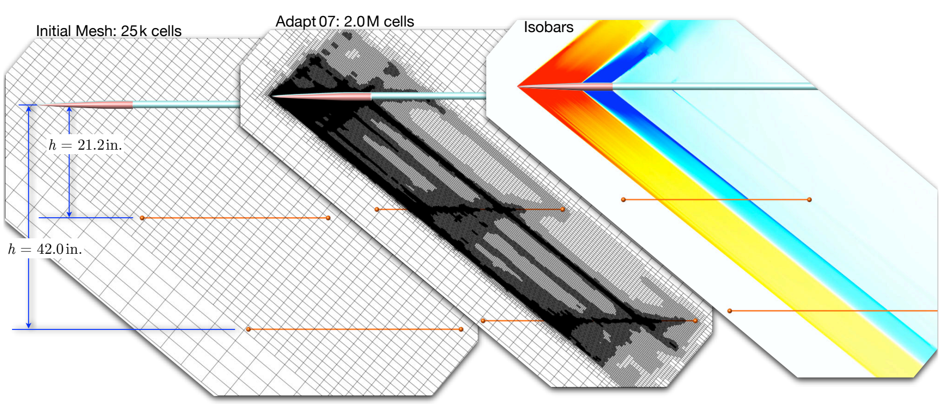

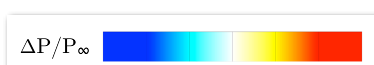

Seeb-ALR: Computational Work

$M_\infty = 1.6, \alpha = 0°$, On-track @ $h = 21.2$ in. & 42 in.

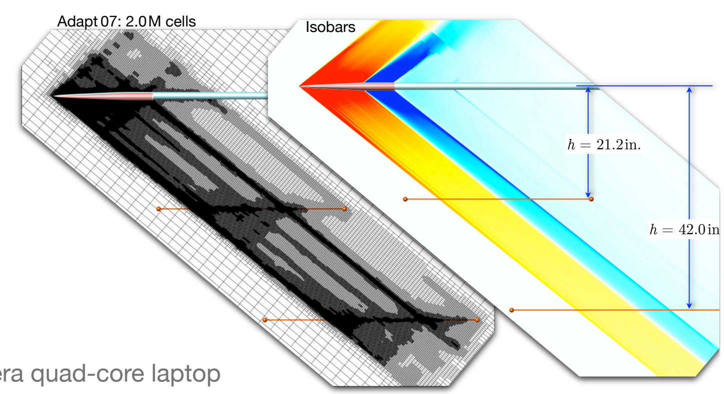

Resources

- Run on 2011-era quad-core laptop
- ~1 hr runtime (61mins)
- 3.6 GB of memory (max)

Seeb-ALR: Mesh Convergence

Convergence of pressure signature, $M_\infty = 1.6$, $\alpha = 0°$

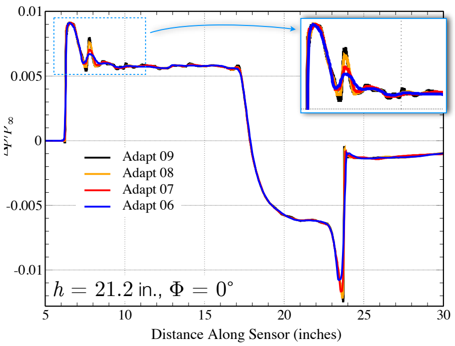

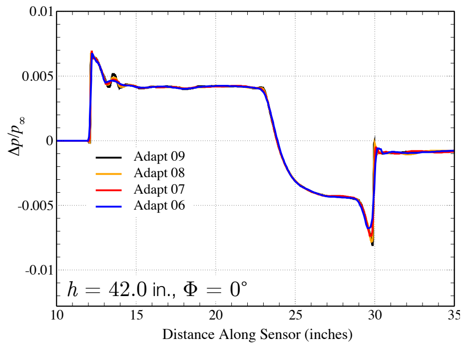

- Pressure signatures largely converged by 6th adapt cycle. - even at 42 in.
- Additional mesh resolution only sharpening shocks

Seeb-ALR: Mesh Convergence

- Results at 7th adaptation submitted to workshop
- Perform 2 more adaptations to assess degree of mesh convergence

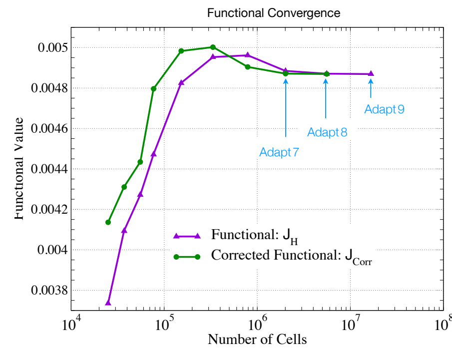

- Functional converges
- Correction *leads* functional
- Adjoint correction vanishes

Seeb-ALR: Mesh Convergence

- Results at 7th adaptation submitted to workshop
- Perform 2 more adaptations to assess degree of mesh convergence

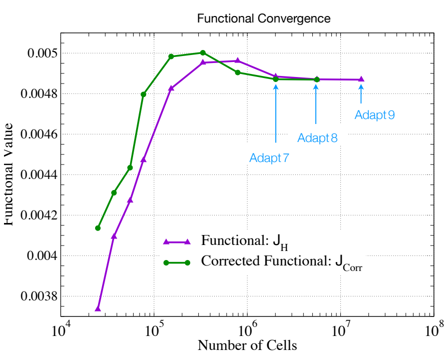

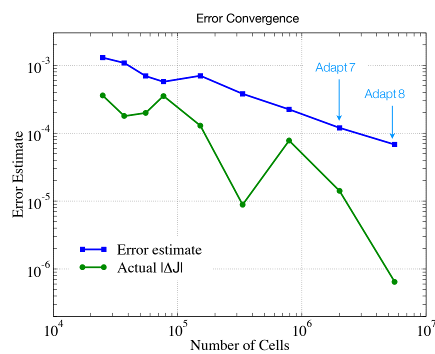

- Functional converges
- Correction *leads* functional
- Adjoint Correction vanishes
- Error-estimate bounds update |ΔJ|
- Remaining error converges asymptotically
- “Textbook” convergence

Seeb-ALR: Data Comparison

Comparison with linear theory, $M_\infty = 1.6$, $\alpha = 0°$

- Code-to-Code comparison used before exp. data was available

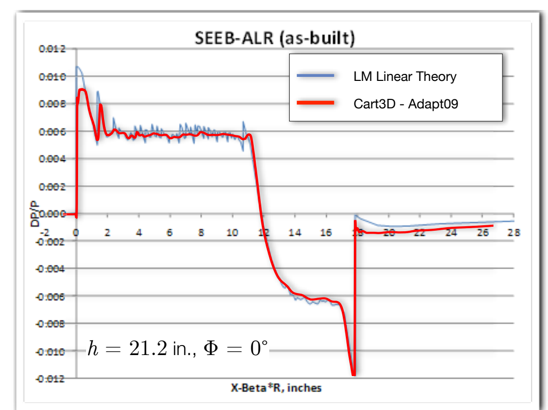

Morgenstern *et al.*, NASA CR–2013-217820, fig 18

Seeb-ALR: Data Comparison

Comparison with experimental data, $M_\infty = 1.6$, $\alpha = 0°$

- Closest data at $h \approx 20.6$ in., $\alpha = -0.3°$, $\beta = -0.3°$
- Excellent agreement in peaks and on flat-top, some differences in expansion

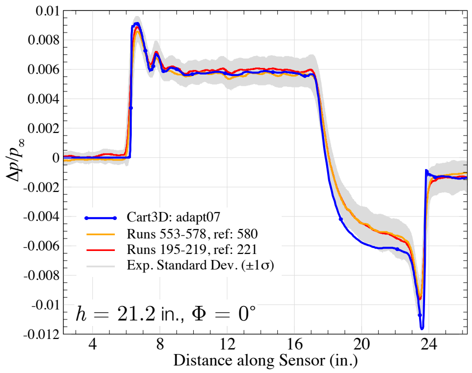

Seeb-ALR: Data Comparison

Compari

- Closes
- Excelle in expans

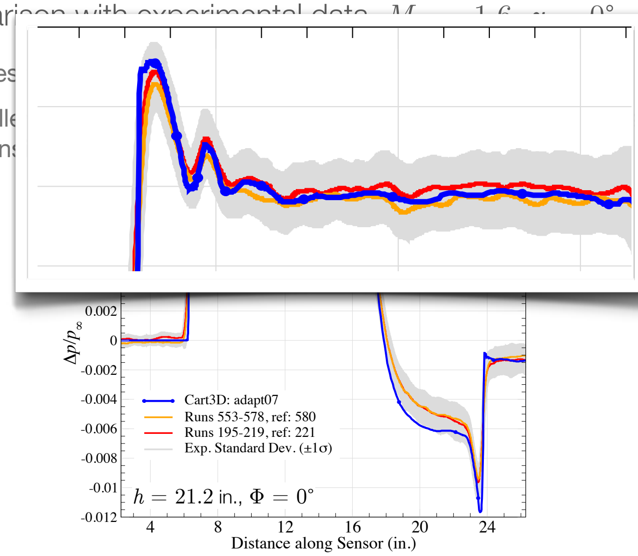

Seeb-ALR: Data Comparison

Comparison with experimental data, $M_\infty = 1.6$, $\alpha = 0°$

- Closest data at $h \approx 20.6$ in., $\alpha = -0.3°$, $\beta = -0.3°$
- Excellent agreement in peaks and on flat-top, some differences in expansion

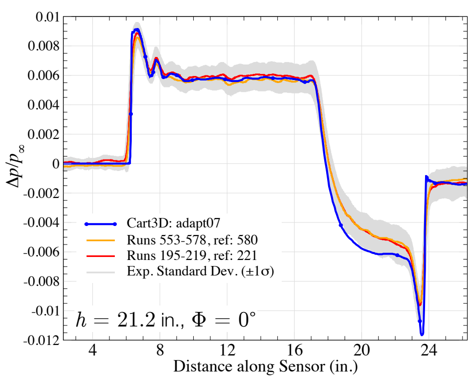

Seeb-ALR: Data Comparison

Comparison with experimental data, $M_\infty = 1.6$, $\alpha = 0°$

- Closest data at $h \approx 20.6$ in., $\alpha = -0.3°$, $\beta = -0.3°$
- Excellent agreement in peaks and on flat-top, some differences in expansion

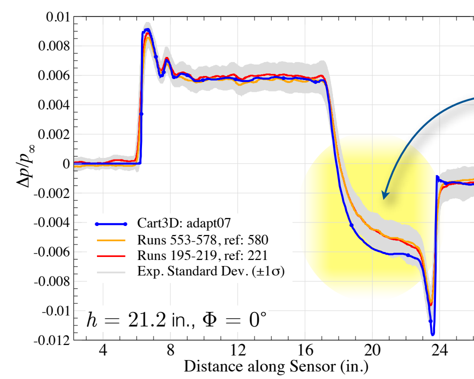

Differences in expansion were troubling since we have high confidence in solution

Seeb-ALR: Data Comparison

Comparison with experimental data, $M_\infty = 1.6$, $\alpha = 0°$

- Closest data at $h \approx 20.6$ in., $\alpha = -0.3°$, $\beta = -0.3°$
- Excellent agreement in peaks and on flat-top, some differences in expansion

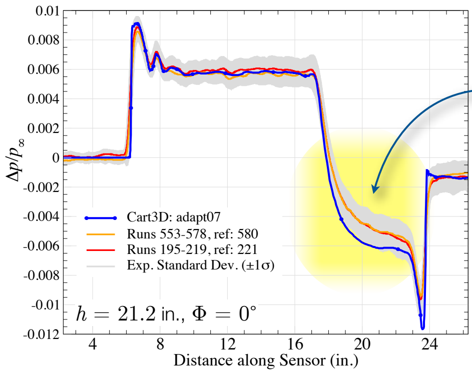

Differences in expansion were troubling since we have high confidence in solution

1. Re-measured model
2. Ran case with Seeb-ALR + pressure rail + tunnel wall

Seeb-ALR: Data Comparison

Simulation with Seeb-ALR + pressure rail + tunnel floor
Mid-traverse location for data @ $h = 20.6$ in.

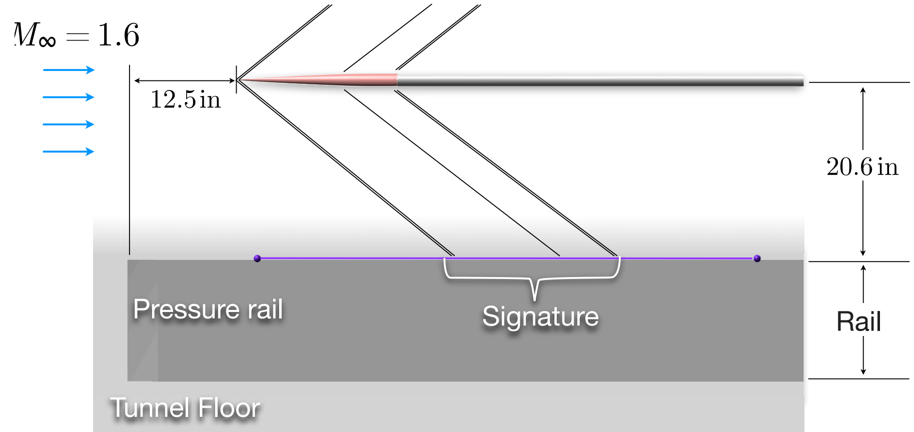

Seeb-ALR: Data Comparison

Simulation with Seeb-ALR + pressure rail + tunnel floor
Mid-traverse location for data @ $h = 20.6$ in.

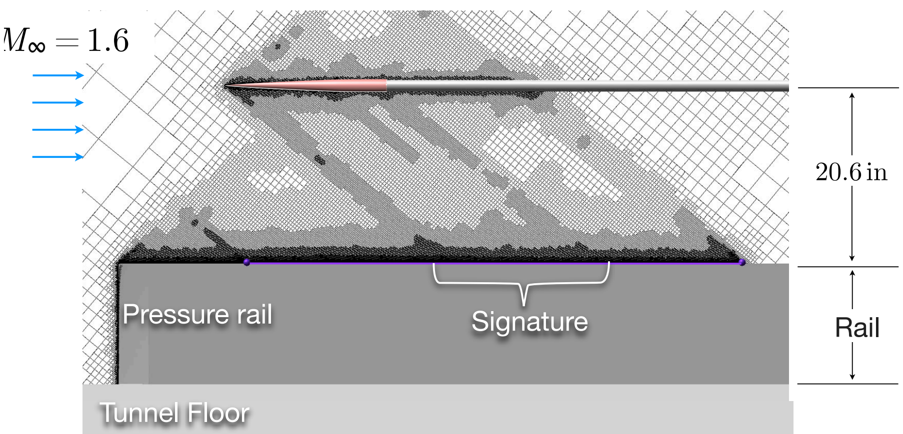

Seeb-ALR: Data Comparison

Simulation with Seeb-ALR + pressure rail + tunnel floor
Mid-traverse location for data @ $h = 20.6$ in.

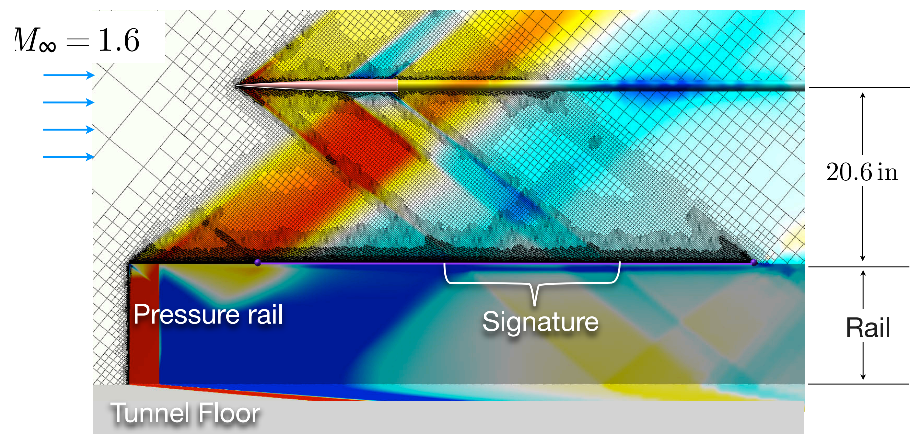

Seeb-ALR: Data Comparison

Simulation with Seeb-ALR + pressure rail + tunnel floor
Mid-traverse location for data @ $h = 20.6\,\mathrm{in.}$

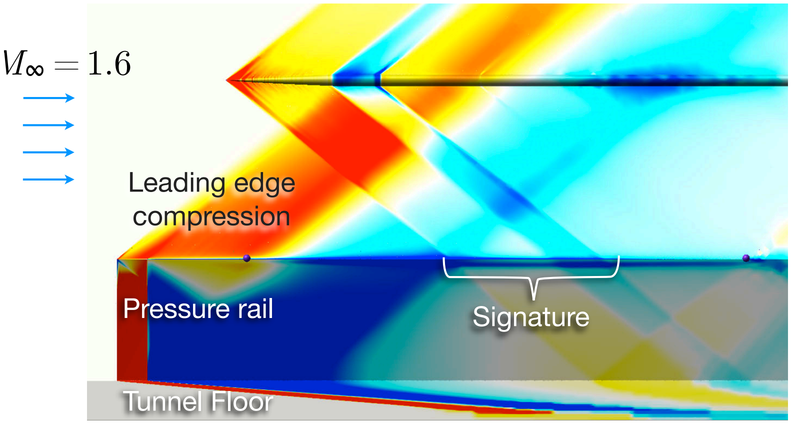

- Model positioned in middle of range of experimental traverse
- Leading edge compression interacts with model, relieving suction

Seeb-ALR: Data Comparison

Simulation with Seeb-ALR + pressure rail + tunnel floor
Mid-traverse location for data @ $h = 20.6\,\mathrm{in.}$

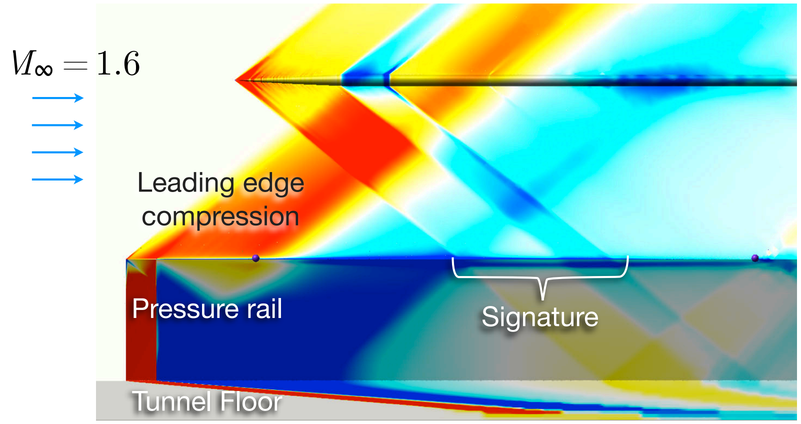

- Model positioned in middle of range of experimental traverse
- Leading edge compression interacts with model, relieving suction

Seeb-ALR: D

Simulation with See
Mid-traverse locatio

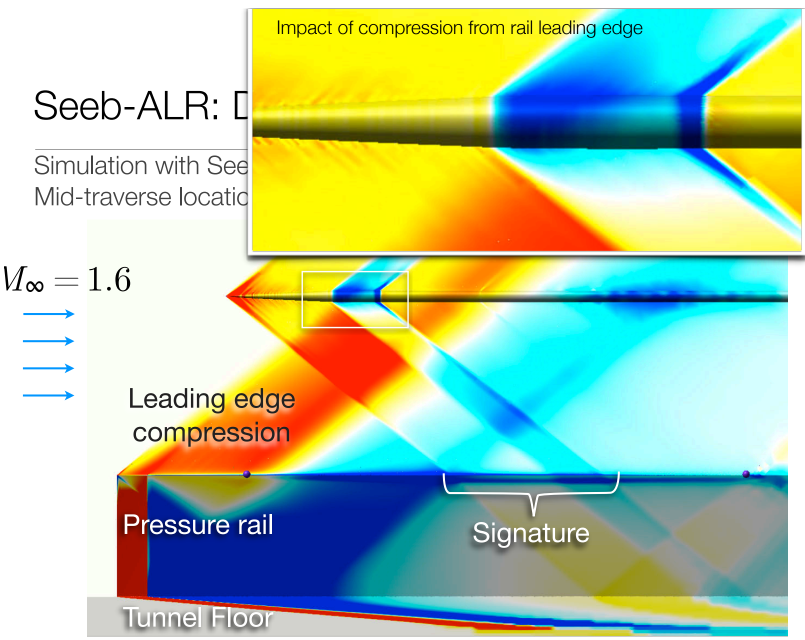

- Model positioned in middle of range of experimental traverse
- Leading edge compression interacts with model, relieving suction

Seeb-ALR: Data Comparison

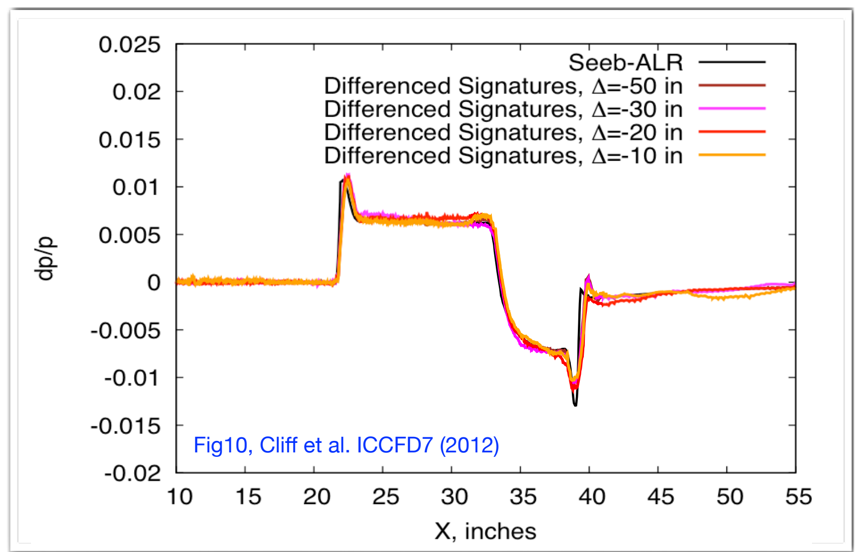

Seeb n

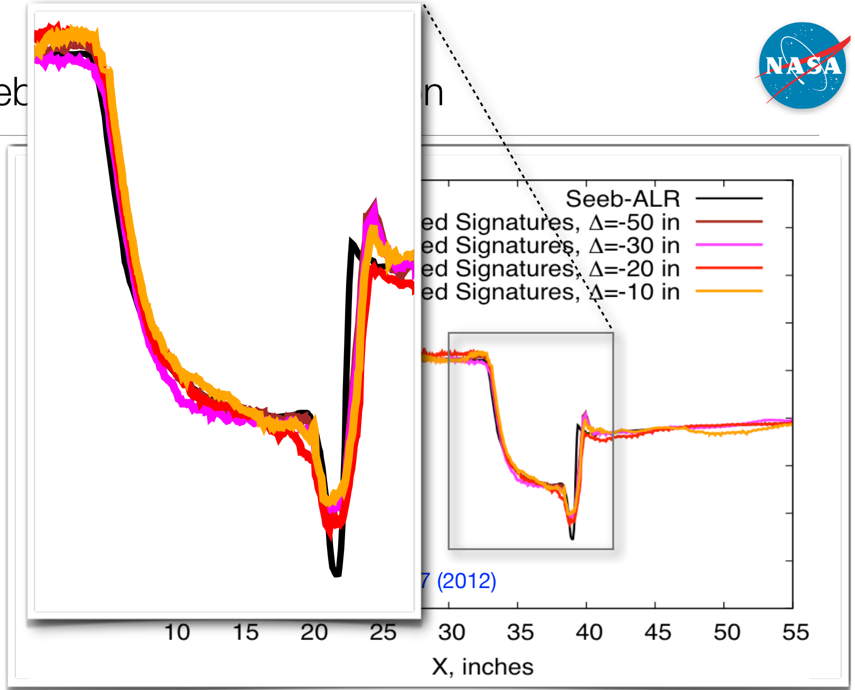

69° Delta Wing Body

$M_\infty = 1.7,\ \alpha = 0^\circ$

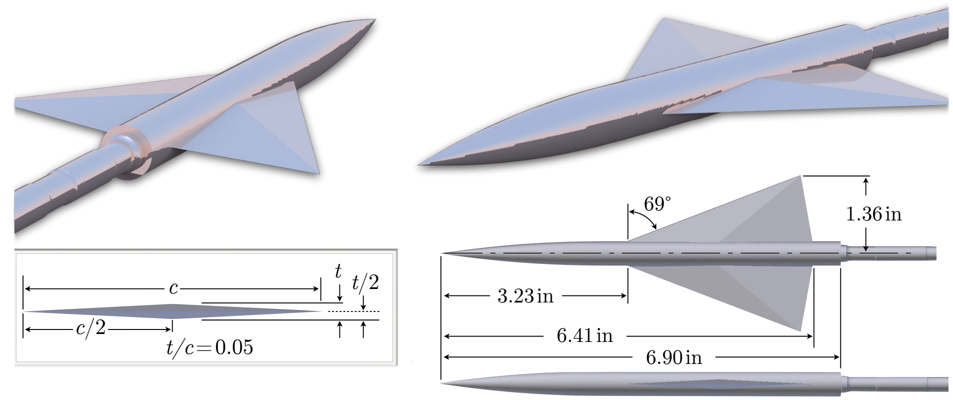

- Tangent-ogive-cylinder fuselage
- Delta wing with 5% thick diamond airfoil
- New sting fitted to original (1973) model from Hunton et al.

69° Delta Wing Body

$M_\infty = 1.7,\ \alpha = 0^\circ$

Required Pressure Signatures

- $\Phi = \{0^\circ, 30^\circ, 60^\circ, 90^\circ\}$
- $h = \{0.5, 21.2, 24.8, 31.8\}$ in.
- 10 sensors, including extreme off-track angles

69° Delta Wing Body

$M_\infty = 1.7$

$\alpha = 0^\circ$

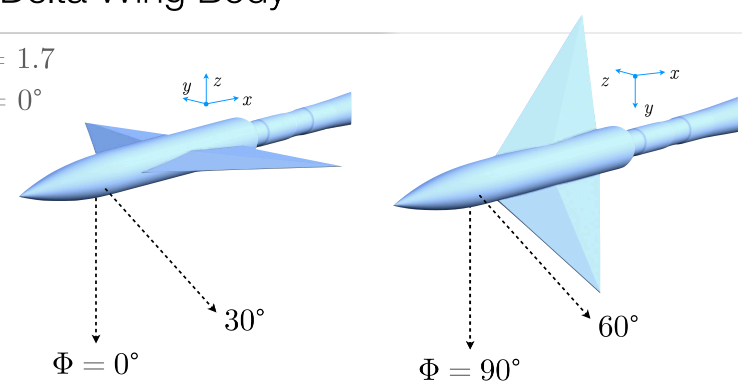

Setup as 2 cases

1. $\Phi = \{0^\circ, 30^\circ\}$ – Mesh rotated in pitch plane
2. $\Phi = \{60^\circ, 90^\circ\}$ – Mesh rotated in yaw plane

Case 2 – 69° Delta Wing Body

$M_\infty = 1.7$
$\alpha = 0°$

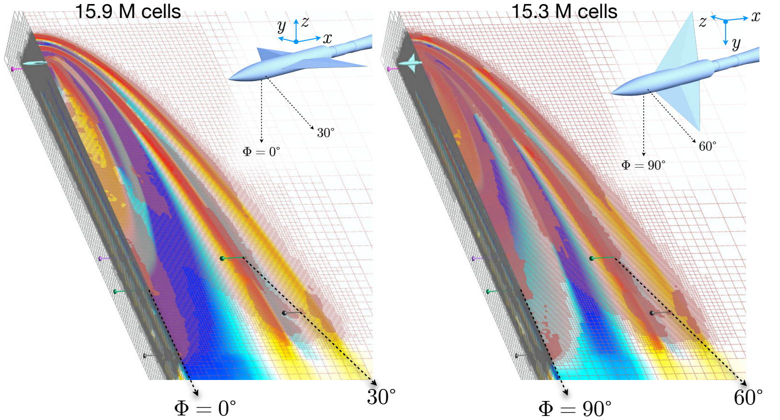

Setup as 2 cases

1. $\Phi = \{0°, 30°\}$ – Mesh rotated in pitch plane
2. $\Phi = \{60°, 90°\}$ – Mesh rotated in yaw plane

Case 2 – 69° Delta Wing Body

$M_\infty = 1.7$
$\alpha = 0°$

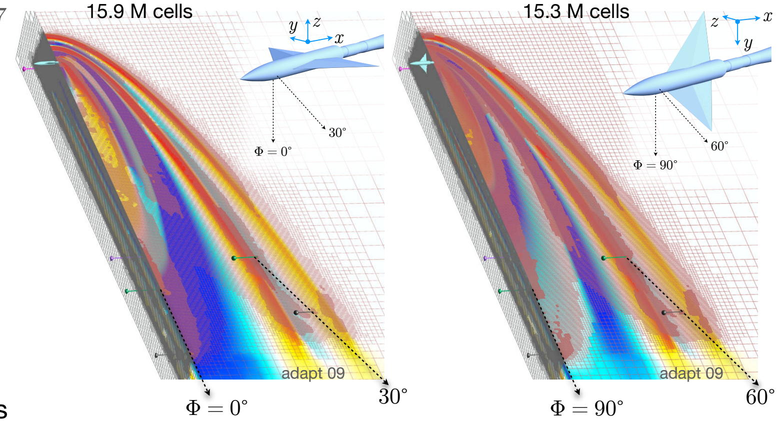

Resources

- Run on dual socket system w/ 20 cores
- (1 hr runtime) x 2
- 36 GB of memory (max)

69° Delta Wing Body: Mesh Convergence

- Results at 9th adaptation submitted to workshop
- Perform 2 more adaptations to assess degree of mesh convergence

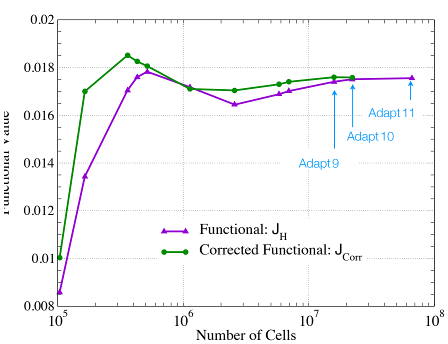

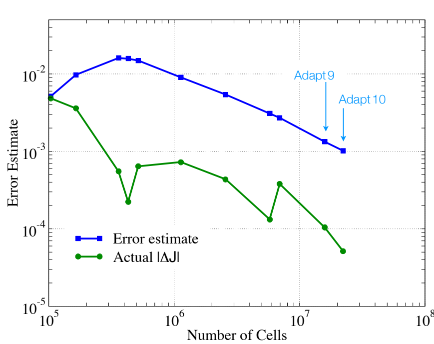

- Functional converges
- Correction *leads* functional
- Adjoint Correction vanishes

- Error-estimate bounds update |ΔJ|
- Remaining error converges asymptotically
- Very good convergence

69° Delta Wing Body: Signatures @ 24.8 in

$M_\infty = 1.7, \alpha = 0°$

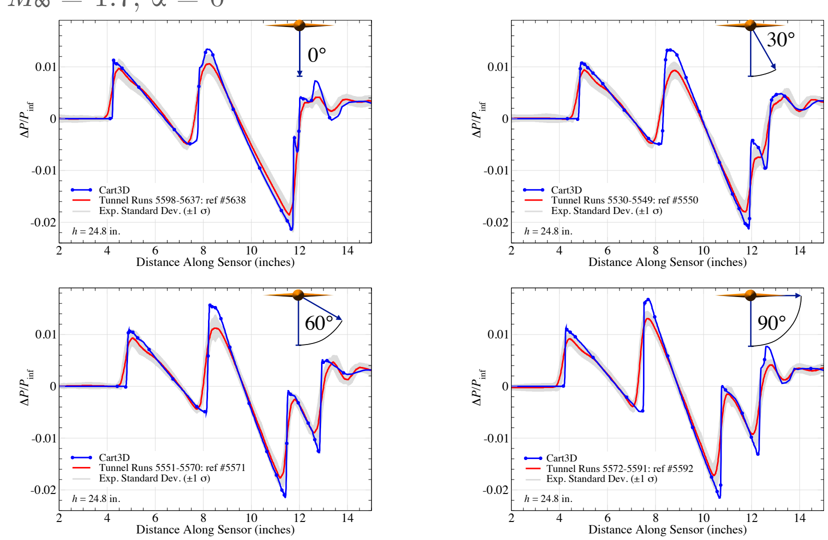

69° Delta Wing Body: Signatures @ 31.8 in

$M_\infty = 1.7,\ \alpha = 0°$

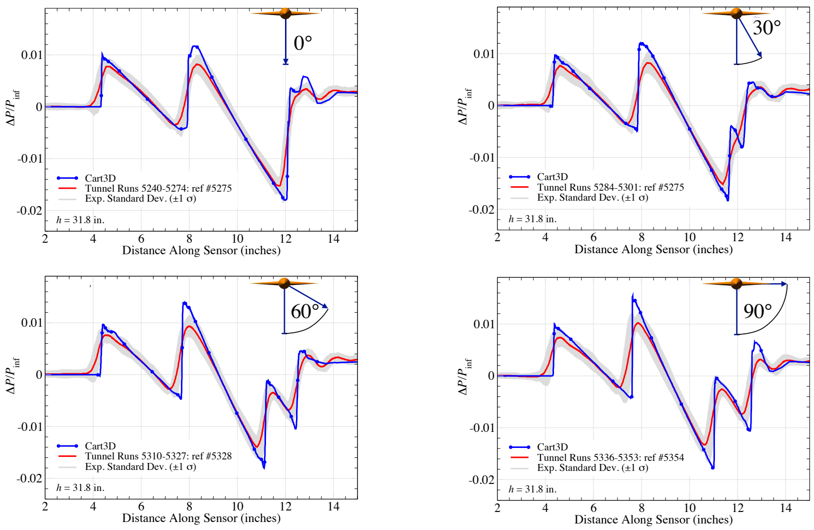

Lockheed Martin LM 1021

$M_\infty = 1.6,\ \alpha = 2.1°$

$L_{ref} = 22.40$ in
$S_{ref} = 33.18$ in^2
$M_\infty = 1.6$
$\alpha_{cruise} = 2.3°$
$C_{L\ cruise} = 0.142$

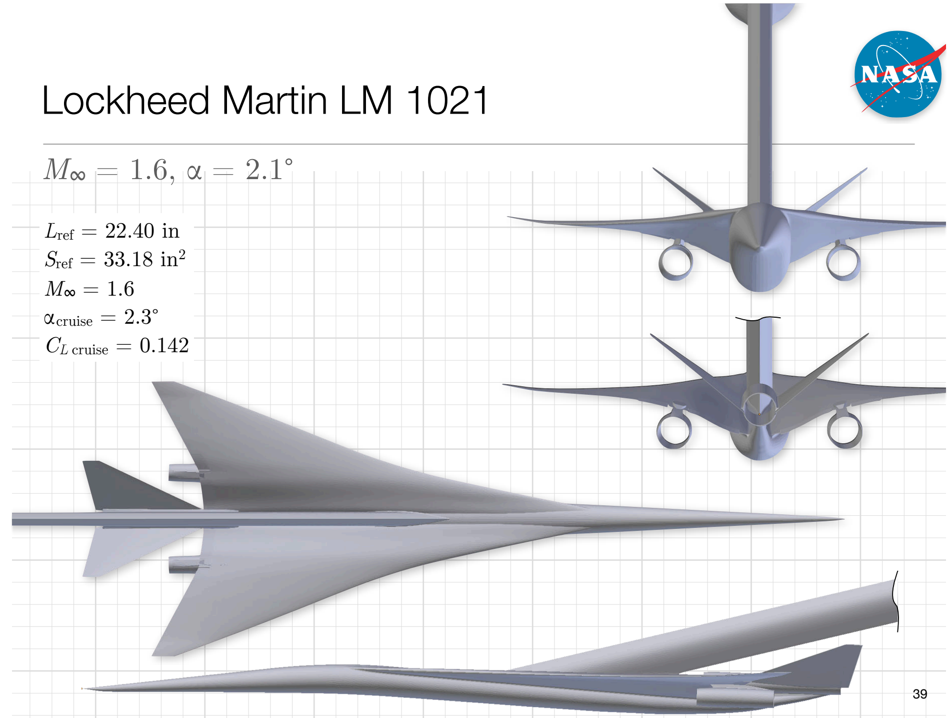

LM 1021: Conditions

$M_\infty = 1.6,\ \alpha = 2.1°$

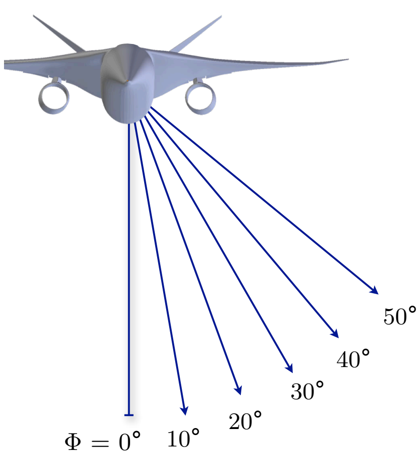

Extracted signatures at 30 locations

- $h = \{1.64, 2.65, 3.50, 5.83, 8.39\}$ ft
- $\Phi = \{0°, 10°, 20°, 30°, 40°, 50°\}$
- Single simulation for all 30 signatures
- Net functional is combination of 30 sensors

$$\mathcal{J} = \sum_{i=1}^{M} w_i \mathcal{J}_i \qquad \text{with}$$

$$w_i = \frac{h_i}{L_{ref}}\left(1 + \frac{4}{\sqrt{2}} \sin \Phi_i\right)$$

Weighting accounts for

- Decrease in signal strength w/ increasing h
- Increase in resolution requirements with increasing Φ
- Goal is to equilibrate contributions of each sensor to the net functional

LM 1021: Meshing

$M_\infty = 1.6,\ \alpha = 2.1°$

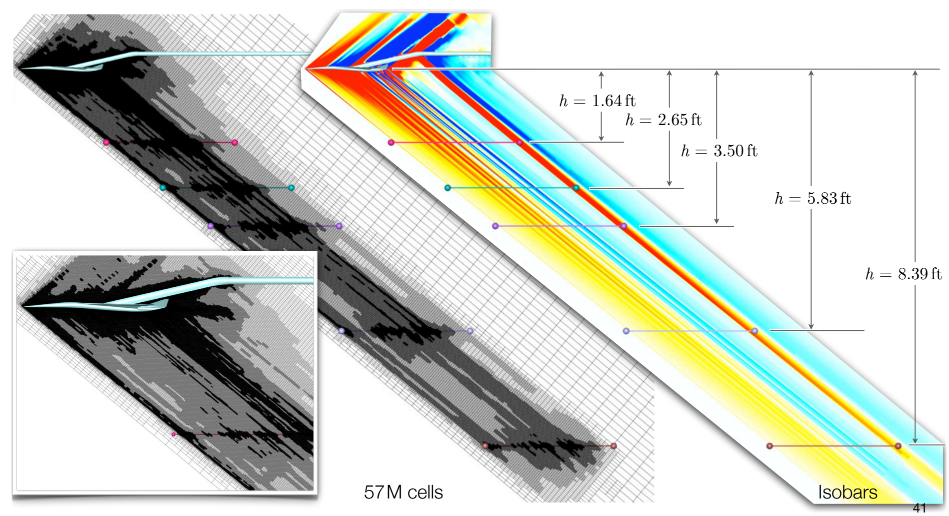

LM 1021: Meshing

$M_\infty = 1.6,\ \alpha = 2.1°$

Isobars and mesh near body

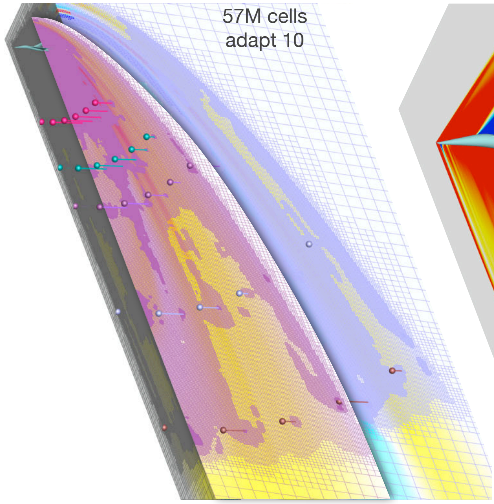

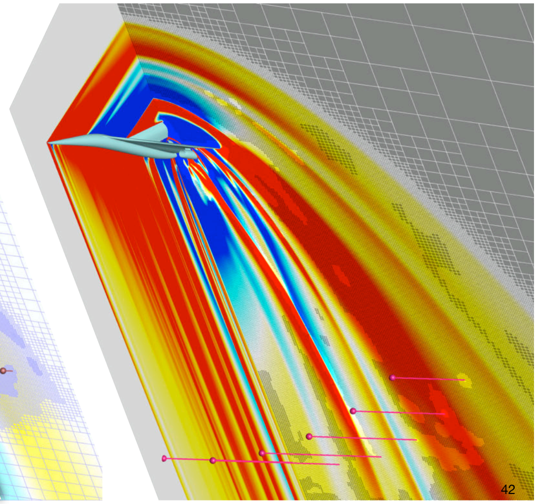

LM 1021: Resources

$M_\infty = 1.6,\ \alpha = 2.1°$

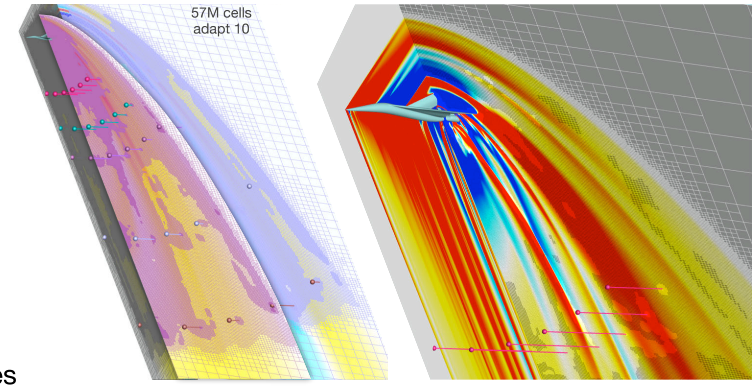

Resources

- Run on 96 Intel sandy bridge cores (NAS's Endeavour system)
- 2 hr 20 mins runtime (61 mins)
- 80 GB of memory (max)

LM 1021: Functional Convergence

- Results at 10th adaptation submitted to workshop
- Perform 1 more adaptations to assess degree of mesh convergence

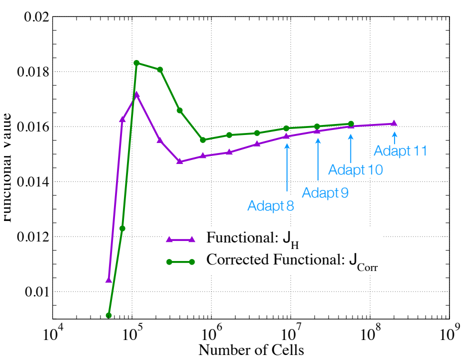

- Functional converges
- Correction *leads* functional
- Adjoint Correction vanishes

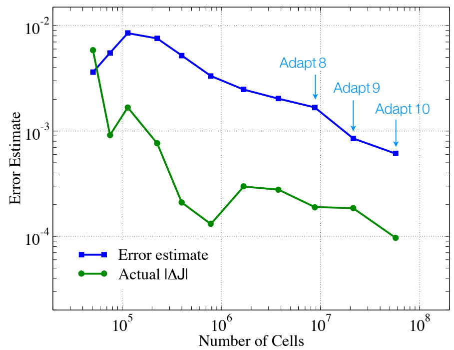

- Error-estimate bounds update |ΔJ|
- Remaining error converges asymptotically
- Very good convergence

LM 1021: Pressure field

$M_\infty = 1.6,\ \alpha = 2.1°$

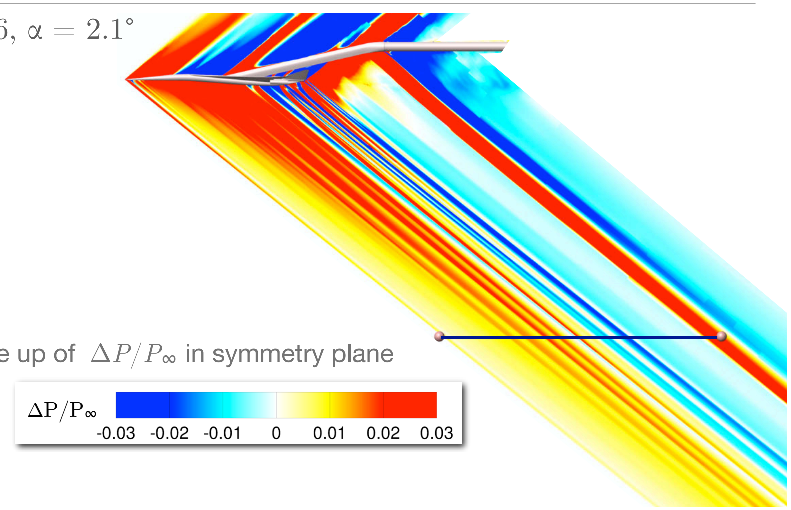

Close up of $\Delta P/P_\infty$ in symmetry plane

LM 1021: Pressure field

$M_\infty = 1.6,\ \alpha = 2.1^\circ$

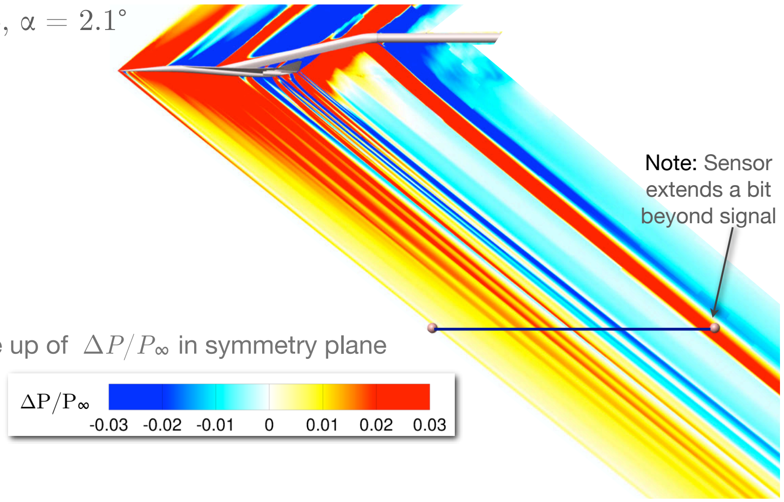

Close up of $\Delta P/P_\infty$ in symmetry plane

LM 1021: Pressure Carpets

$M_\infty = 1.6,\ \alpha = 2.1^\circ$

- h = {1.64, 2.65, 3.50, 5.83, 8.39} ft
- $\Phi = \{0^\circ, 10^\circ, 20^\circ, 30^\circ, 40^\circ, 50^\circ\}$
- Construct pressure carpets by tessellating data along sensors at fixed h/L

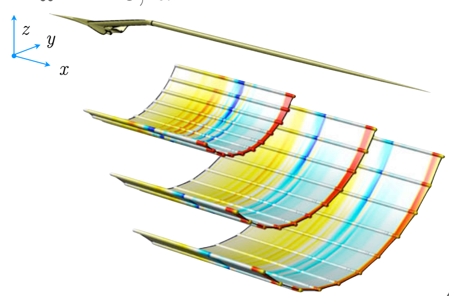

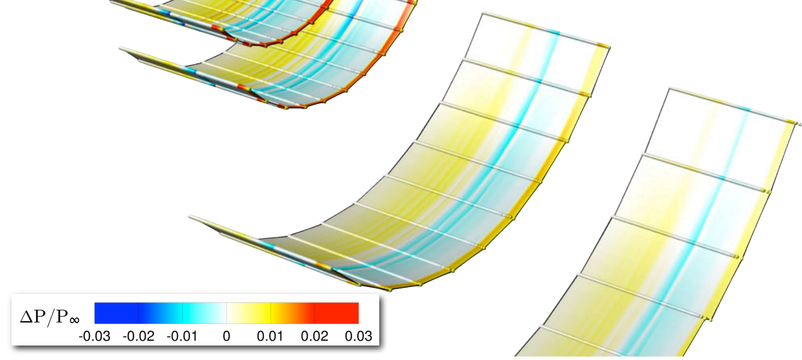

LM 1021: Pressure Carpets

$M_\infty = 1.6,\ \alpha = 2.1^\circ$

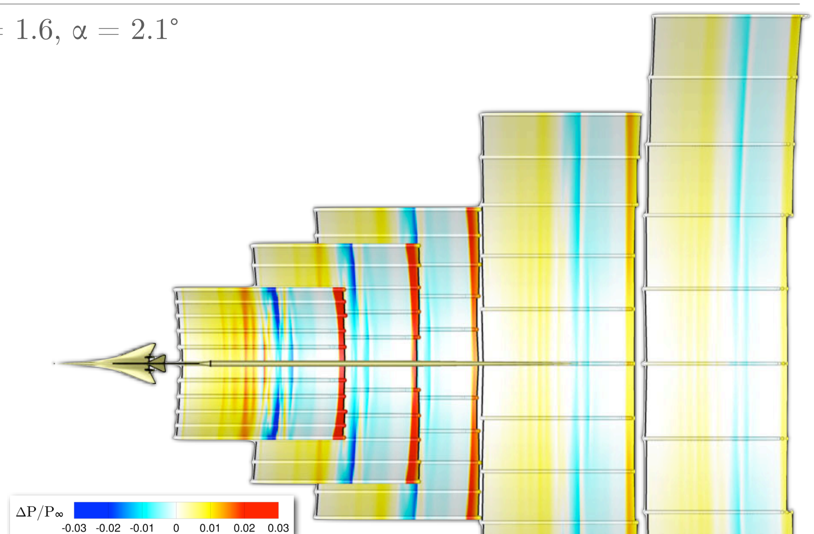

Top-down view of pressure carpets

LM 1021: Pressure Carpets

$M_\infty = 1.6,\ \alpha = 2.1^\circ$

- Appears very quiet on-track

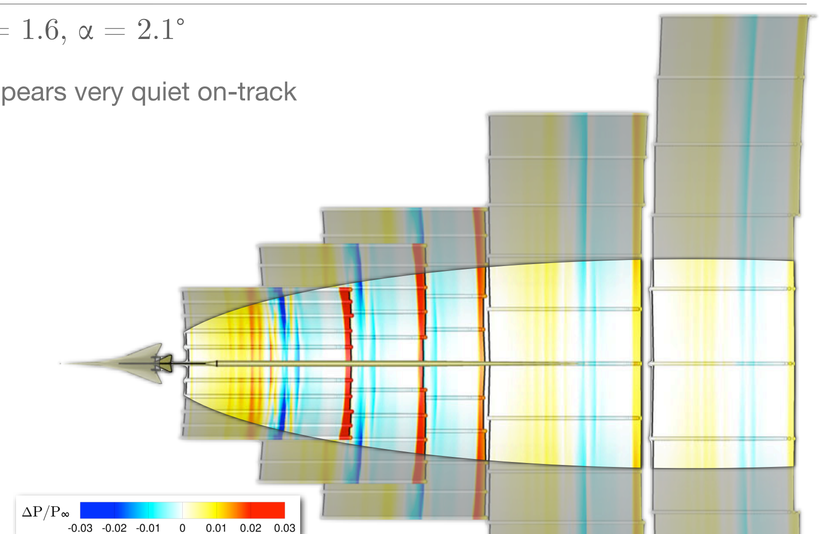

Top-down view of pressure carpets

LM 1021: Pressure Carpets

$M_\infty = 1.6,\ \alpha = 2.1°$

- Appears very quiet on-track
- Strong expansion off-track @ Φ > 10°-15°
- Persists at large h and Φ

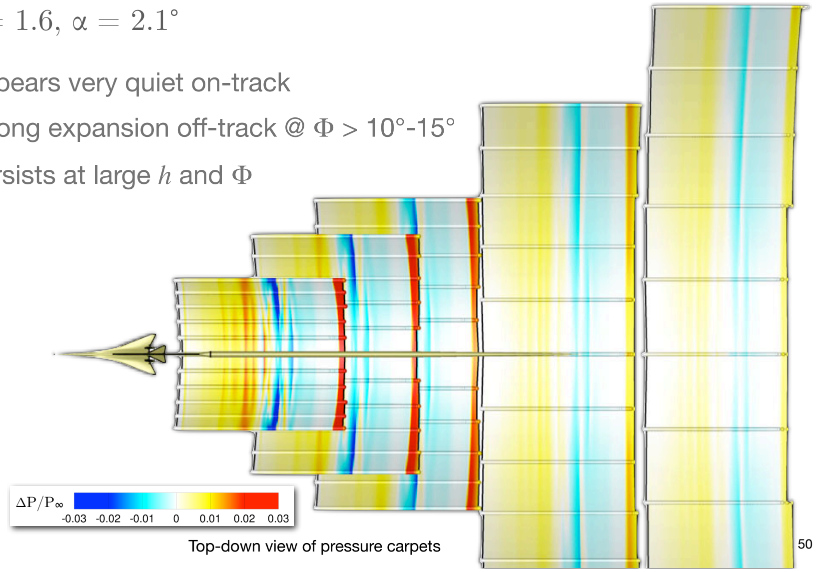

Top-down view of pressure carpets

LM 1021: Off-track Pressure Signature

$M_\infty = 1.6,\ \alpha = 2.1°,\ \Phi = 50°$

- Good agreement
- Difference in alpha may account for the slightly lower peaks

Experimental data at α = 2.3° & Φ = 47°

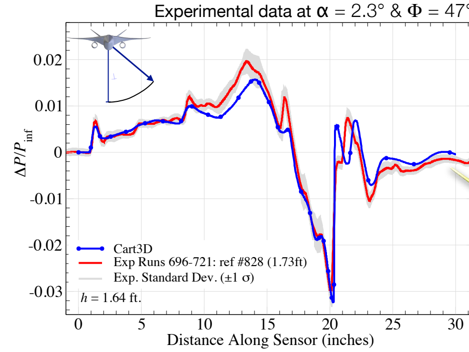

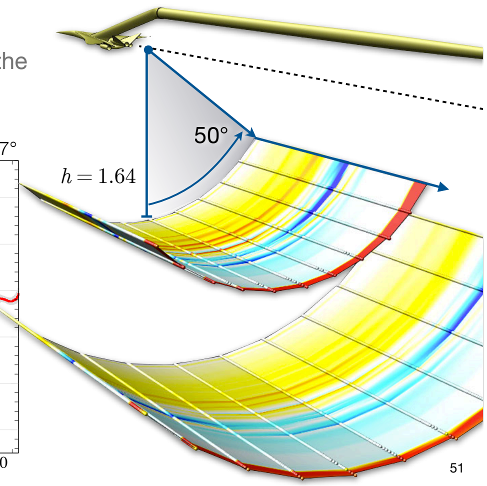

LM 1021: Off-track Pressure Signature

$M_\infty = 1.6,\ \alpha = 2.1°,\ \Phi = 20°$

Experimental data at α = 2.3°

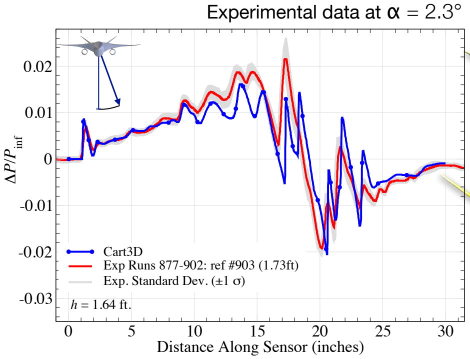

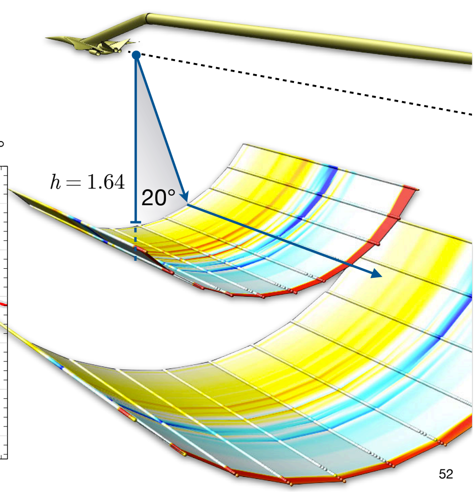

LM 1021: On-track Pressure Signature

$M_\infty = 1.6,\ \alpha = 2.1°,\ \Phi = 0°$

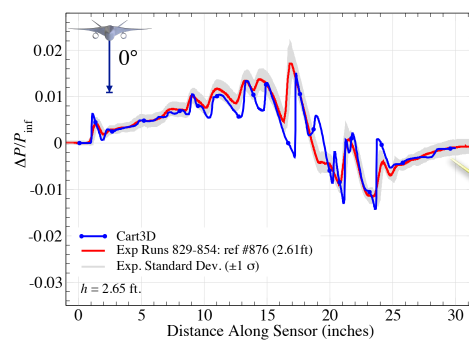

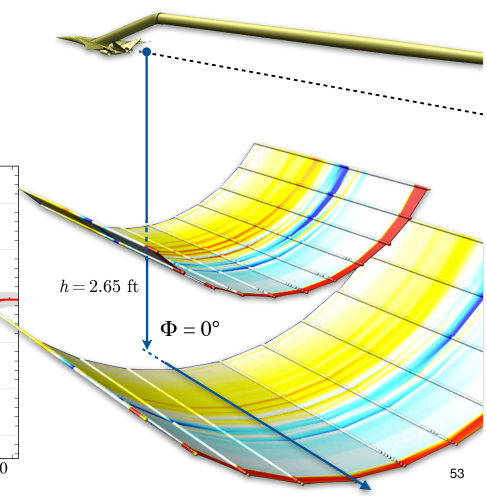

LM 1021: Investigation of On-track Discrepancy

Surprising, since comparisons with RANS at flight Reynolds number was much better!

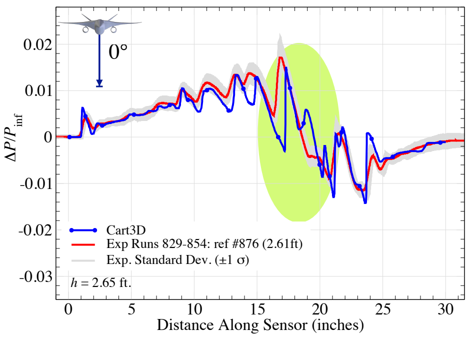

LM 1021: Investigation of On-track Discrepancy

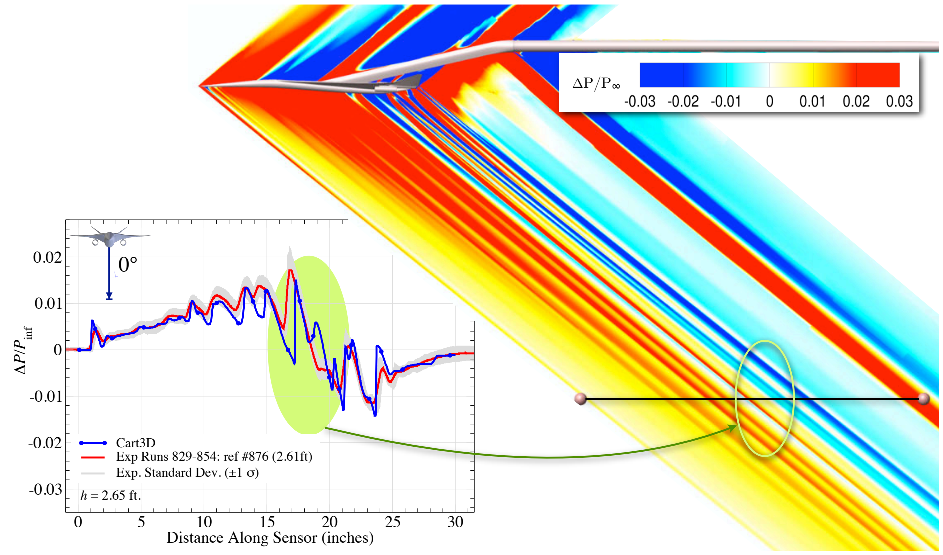

LM 1021: Investigation of On-track Discrepancy

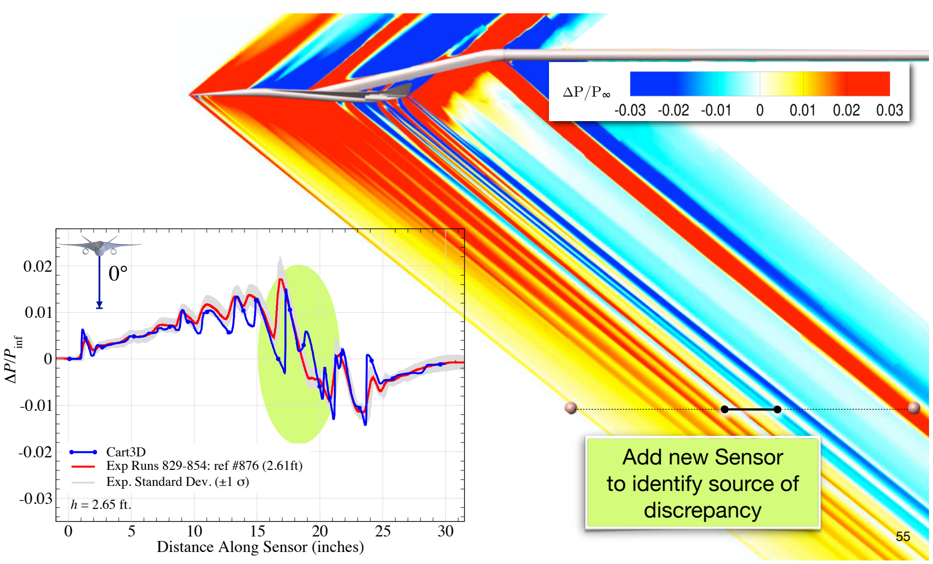

LM 1021: Investigation of On-track Discrepancy

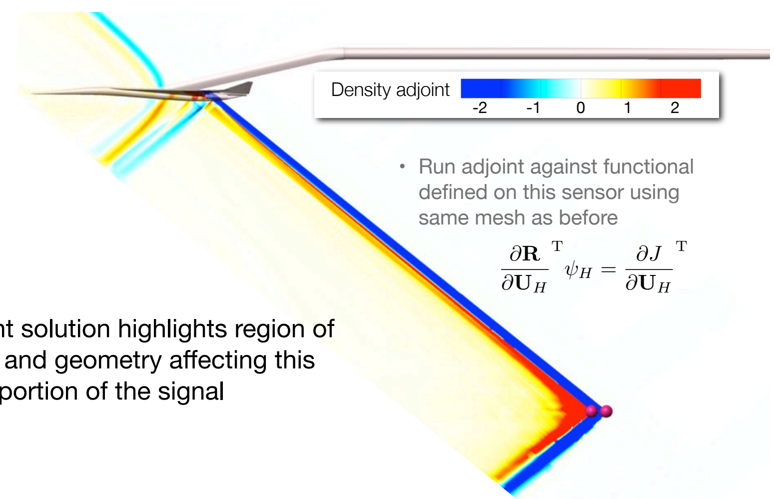

- Run adjoint against functional defined on this sensor using same mesh as before

$$\frac{\partial \mathbf{R}}{\partial \mathbf{U}_H}^T \psi_H = \frac{\partial J}{\partial \mathbf{U}_H}^T$$

The adjoint solution highlights region of the flow and geometry affecting this portion of the signal

LM 1021: Investigation of On-track Discrepancy

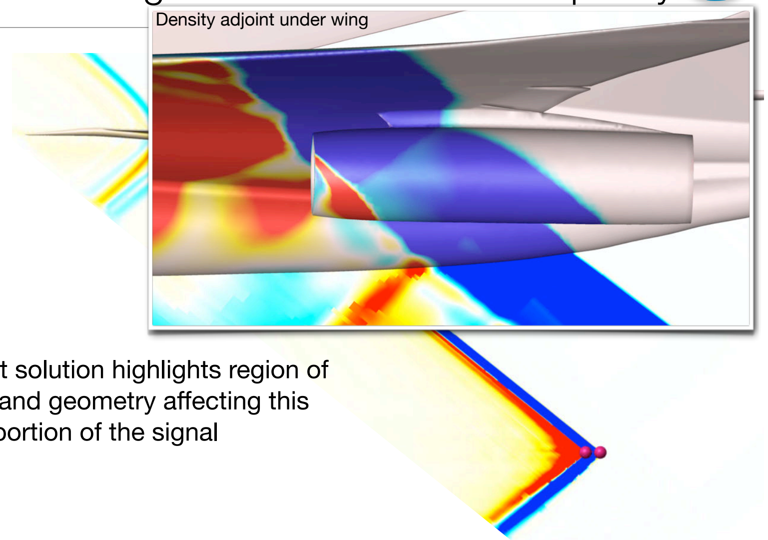

The adjoint solution highlights region of the flow and geometry affecting this portion of the signal

LM 1021: Investigation of On-track Discrepancy

- Adjoint tells us where to look...
- Investigate physics of tunnel flow

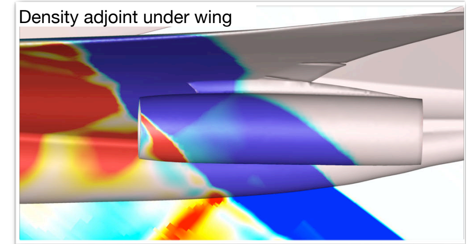

LM 1021: Investigation of On-track Discrepancy

- Adjoint tells us where to look...
- Investigate physics of tunnel flow
- Viscous results from USM3D
- Tunnel Re_L is ~100x lower than flight
- Boundary layer extends to nacelle

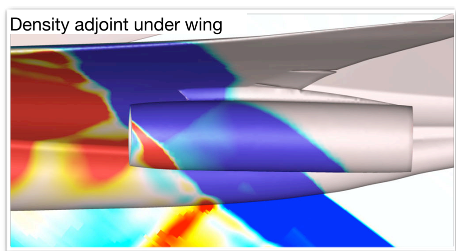

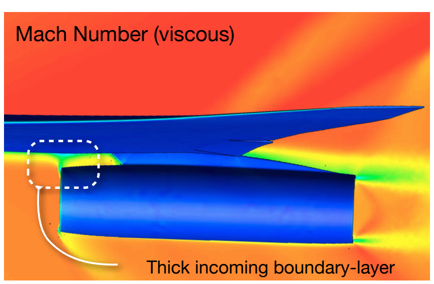

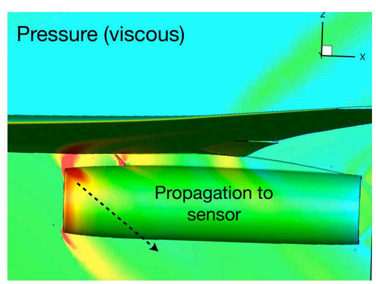

LM 1021: Investigation of On-track Discrepancy

- Compare viscous and inviscid
- Boundary layer extends to nacelle
- Inviscid has supersonic flow between underside of wing and nacelle
- Inviscid shock is delayed (oblique)
- 2nd peak comes from pylon

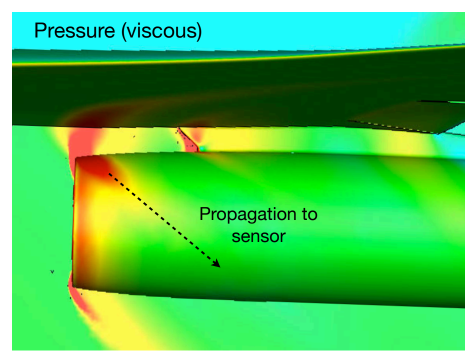

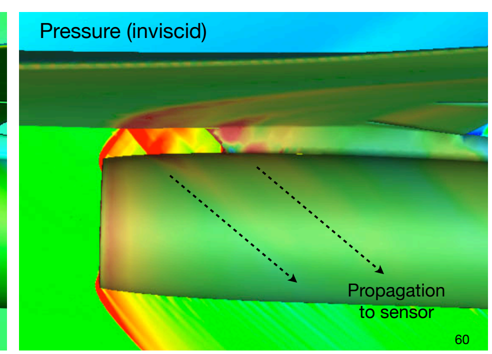

LM 1021: Investigation of

- Compare viscous and inviscid
- Boundary layer extends to nacelle
- Inviscid has supersonic flow between
- Inviscid shock is delayed (oblique)
- 2nd peak comes from pylon

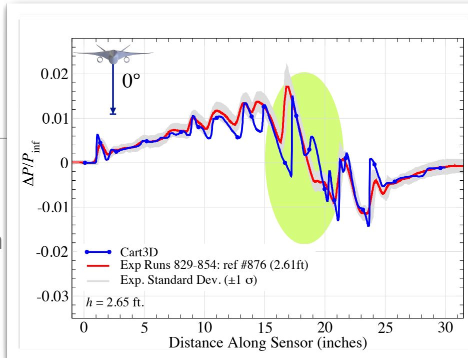

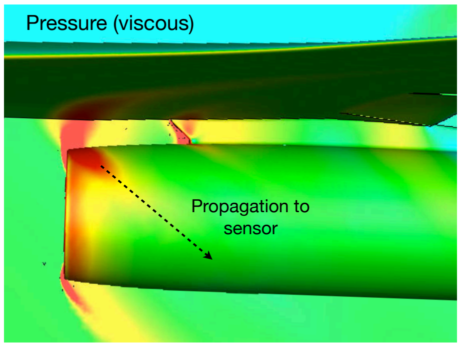

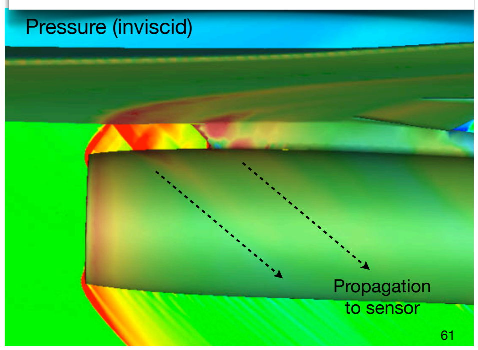

Summary

- Presented results for SEEB-ALR, DWB and LM 1021 using inviscid Cartesian method with
  - Automated meshing & adjoint-driven adaptation used for all cases
  - Presented evidence of mesh convergence
    - (1) Pressure signature
    - (2) Output Functional
    - (3) Adjoint correction and error estimate
  - Computational resources
    - Seeb-ALR: ~1hr on a quad-core laptop in ~3.6 Gb
    - LM 1021: Under 2.5hrs on 96 cores in 80 Gb

Summary

- Presented results for SEEB-ALR, DWB and LM 1021 using inviscid Cartesian method with
  - Automated meshing & adjoint-driven adaptation used for all meshing
  - Presented evidence of mesh convergence
    - (1) Pressure signature
    - (2) Output Functional
    - (3) Adjoint correction and error estimate
  - Computational resources
    - Seeb-ALR: ~1hr on a quad-core laptop in ~3.6 Gb
    - LM 1021: Under 2.5hrs on 96 cores in 80 Gb
- Investigations
  - SEEB-ALR:
    - Showed that differences in main expansion are likely due to influence of rail leading-edge compression impacting shoulder of model
    - Results are consistent w/ earlier studies
  - LM 1021:
    - Good agreement off-track
    - Low tunnel Reynolds number results in differences in on-track signal
    - Showed a powerful technique using the adjoint-solver to trace specific regions of the signature to particular regions of the surface geometry and near-body flow

Summary

- Presented resul
  - Automated m
  - Presented ev
    - (1) Pr
    - (2) O
    - (3) Ad
  - Computation
    - Seeb
    - LM 1

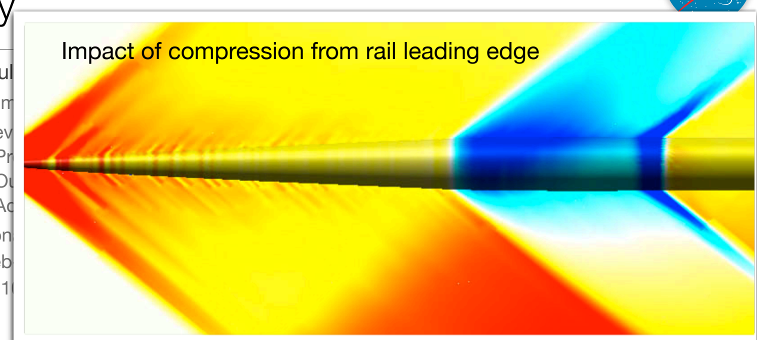

- Investigations
  - SEEB-ALR:
    - Showed that differences in main expansion are likely due to influence of rail leading-edge compression impacting shoulder of model
    - Results are consistent w/ earlier studies
  - LM 1021:
    - Good agreement off-track
    - Low tunnel Reynolds number results in differences in on-track signal
    - Showed a powerful technique using the adjoint-solver to trace specific regions of the signature to particular regions of the surface geometry and near-body flow

Summary

- Presented results for SEEB-ALR, DWB and LM 1021 using inviscid Cartesian method with
  - Automated meshing & adjoint-driven adaptation used for all meshing
  - Presented evidence of mesh convergence
    (1) Pressure signature
    (2) Output Functional
    (3) Adjoint correction and error estimate
  - Computational resources
    - Seeb-ALR: ~1hr on a quad-core laptop in ~3.6 Gb
    - LM 1021: Under 2.5hrs on 96 cores in 80 Gb
- Investigations
  - SEEB-ALR:
    - Showed that differences in main expansion are likely due to influence of rail leading-edge compression impacting shoulder of model
    - Results are consistent w/ earlier studies
  - LM 1021:
    - Good agreement off-track
    - Low tunnel Reynolds number results in differences in on-track signal
    - Showed a powerful technique using the adjoint-solver to trace specific regions of the signature to particular regions of the surface geometry and near-body flow

Thanks!

- Fundamental Aeronautics High Speed Project for support & leadership
- Workshop Organizing committee
- Susan Cliff, Don Durston, David Rodriguez and Mathias Wintzer

Questions?

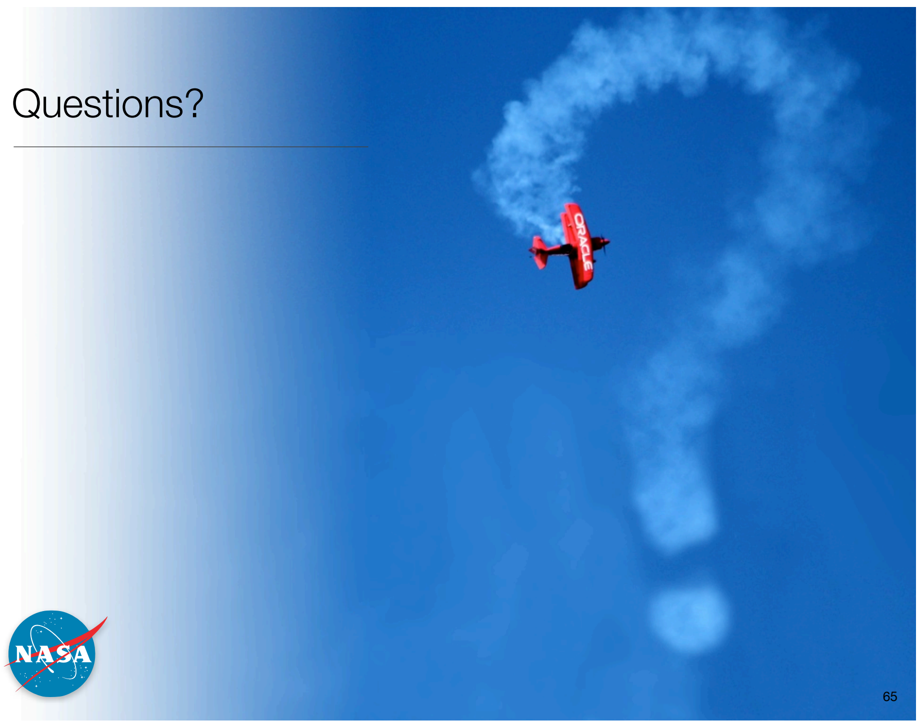

Backup

Seeb-ALR: Data Comparison

Comparison with experimental data, $M_\infty = 1.6$, $\alpha = 0°$

Tunnel Runs	Reference Run	M_∞	α	β	Altitude, h
553-578	#580	1.6	-0.27°	0.17°	20.62 in.
195-219	#221	1.6	-0.29°	0.17°	20.59 in.

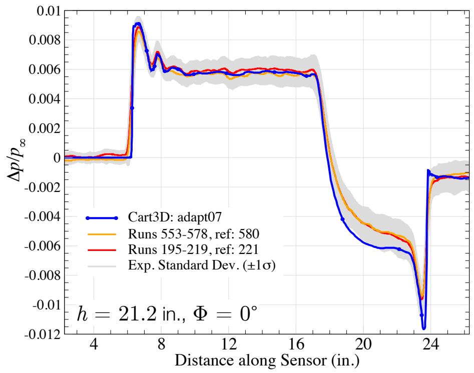

Seeb-ALR: Data Comparison

Comparison with experimental data, M

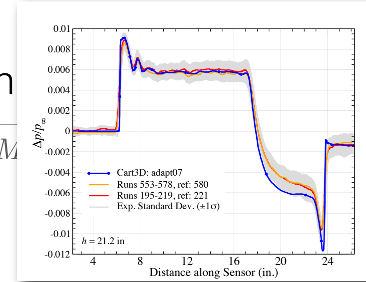

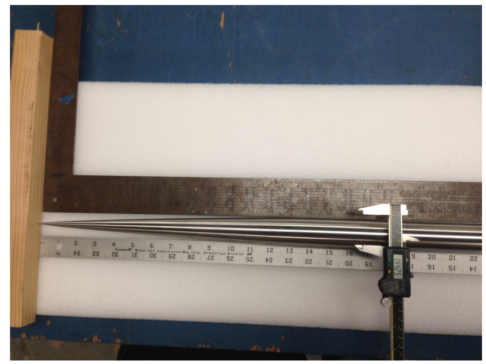

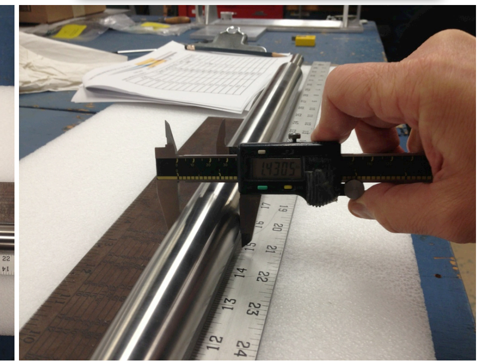

Backup

69° DWB - Tunnel Conditions

Tunnel Runs	Reference Run	M_∞	α	Φ	Altitude, h
5598-5637	#5638	1.7	0.24	0.16°	24.86 in.
5530-5549	#5550	1.7	-0.20	29.97°	24.75 in.
5551-5570	#5571	1.7	-0.18	60.06°	24.75 in.
5572-5591	#5592	1.7	-0.18	89.87°	24.69 in.
5240-5274	#5275	1.7	-0.06	0.60°	31.64 in.
5284-5301	#5275	1.7	-0.17	29.94°	31.74 in.
5310-5327	#5328	1.7	-0.22	59.74°	31.56 in.
5336-5354	#5354	1.7	-0.20	89.96°	31.61 in.

Case 1 – Seeb-ALR

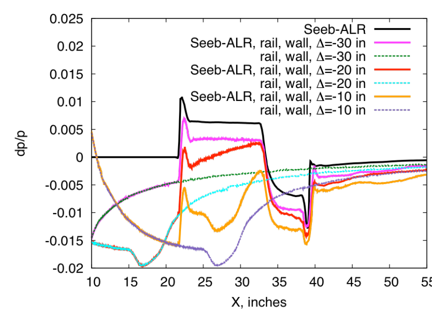

a) Seeb-ALR, RF 1.0 rail, and tunnel wall pressure signatures

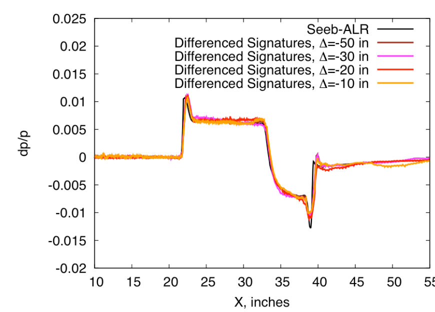

b) Differenced signatures compared to model free-air solution

Backup

69° DWB - Signature Convergence